ACADEMIC PRESS

Available online at www.sciencedirect.com

SCIENCE DIRECT®

Journal of Sound and Vibration 265 (2003) 175–200

JOURNAL OF SOUND AND VIBRATION

www.elsevier.com/locate/jsvi

On the prediction of "buzz-saw" noise in acoustically lined aero-engine inlet ducts

A. McAlpine*, M.J. Fisher

Institute of Sound and Vibration Research, University of Southampton, Southampton SO17 1BJ, UK

Received 7 December 2001; accepted 23 July 2002

Abstract

Aero-engines operating with supersonic fan tip speeds generate an acoustic signature containing energy spread over a range of harmonics of the engine shaft rotation frequency. These harmonics are commonly known as the "buzz-saw" tones. The pressure signature attached to a supersonic ducted fan will be a sawtooth waveform. The non-linear propagation of a high-amplitude irregular sawtooth upstream inside the inlet duct redistributes the energy amongst the buzz-saw tones. In most modern aero-engines the inlet duct contains an acoustic lining, whose properties will be dependent on the mode number and frequency of the sound, and the speed of the oncoming flow. Such effects may not easily be incorporated into a time-domain approach; hence the non-linear propagation of an irregular sawtooth is calculated in the frequency domain, which enables liner damping to be included in the numerical model. Results are presented comparing noise predictions in hard-walled and acoustically lined inlet ducts. These show the effect of an acoustic liner on the buzz-saw tones. These predictions compare favourably with previous experimental measurements of liner insertion loss (at blade passing frequency), and provide a plausible explanation for the observed reduction in this insertion loss at high fan operating speeds.

1. Introduction

Aero-engines operating with fan tip speeds which exceed the speed of sound are known to generate an acoustic signature which contains energy spread over a wide range of harmonics of the engine shaft rotation frequency. Variously referred to as "multiple pure", "combination" or "buzz-saw" tones, this noise source has been a prevalent feature of aircraft noise since the entry into service in the 1970s of higher bypass ratio aircraft engines.

*Corresponding author. Tel.: +44-23-8059-2291; fax: +44-23-8059-3190.
E-mail address: am@isvr.soton.ac.uk (A. McAlpine).

0022-460X/03/$ - see front matter
doi:10.1016/S0022-460X(02)01446-3

Typically the dominant tones generated by a supersonic ducted fan will have frequency less than the blade passing frequency (BPF). Therefore buzz-saw noise is usually identified by its lower pitch, compared with high-pitched tonal noise (BPF harmonics) generated by a subsonic fan. Buzz-saw noise is clearly audible during take-off and climb, and will affect the cabin and community noise levels. This noise source remains a current concern with the advent of larger aircraft engines, the likelihood of more stringent noise regulations and a public demand for lower aircraft noise levels.

Research reported during the 1970s including Refs. [1–6] offered a reasonable explanation of the basic generation and controlling mechanisms of the buzz-saw noise in terms of the non-linear propagation of a high-amplitude irregular sawtooth pressure signature within the engine inlet duct.

The generation of buzz-saw noise is usually described in terms of a simple plane two-dimensional model of the "rotor-alone" pressure field inside the inlet duct of an aero-engine (cf., Fig. 1). The fan is represented by a cascade of rotor blades. The Mach numbers of the uniform inlet flow and rotor blade tips are M_a and M_t, respectively. In a frame of reference rotating with the fan, there will be a flow impinging on the rotor blades with relative Mach number M_{rel}. For $M_{rel} > 1$ the rotor-alone pressure field consists of a series of shock waves and expansion fans, which extend upstream of the fan. The pressure signature in a direction normal to the shock fronts is a sawtooth pressure waveform. On assuming that the flow is only supersonic over a small radial extent, close to the rotor blades' tips, then the sawtooth will be confined radially to a location close to the duct wall. The sawtooth will spiral upstream inside the inlet duct in a helical path.

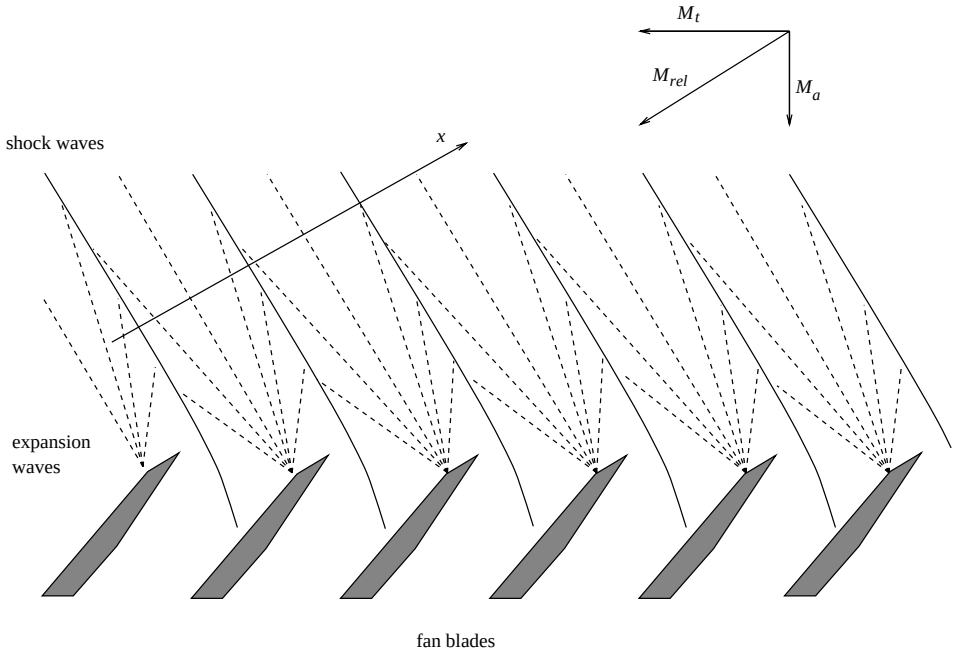

Fig. 1. Shock-wave generation by a supersonic fan (after McAlpine and Fisher [11, Fig. 1]).

Shortly upstream of the fan most of the energy in the sawtooth frequency spectrum is located at harmonics of BPF. Stratford and Newby [6] have shown that close to the fan's leading edge, small variations in the sawtooth waveform are predominantly caused by blade stagger angle variations. There will be energy in the frequency spectrum of an irregular sawtooth at harmonics of the engine shaft rotation frequency $\mathscr{F}$, namely engine orders (EO). The EO harmonics are spinning modes which are steady in a frame of reference rotating with the fan/rotor. In this paper all the EO harmonics (including the BPF harmonics) will be known as the rotor-alone tones, whereas the buzz-saw tones will only specifically refer to the EO harmonics with frequency less than BPF.

The shocks in an irregular sawtooth will propagate at slightly different speeds relative to each other. Therefore, the redistribution of energy between the EO harmonics occurs during the non-linear propagation of the initially high-amplitude sawtooth waveform. By the end of the duct the blade-to-blade periodicity in the sawtooth will be lost, and the dominant energy in the frequency spectrum will typically be located at EOs whose frequencies are less than BPF, i.e., the buzz-saw tones.

There has been less research on the full three-dimensional problem concerning the generation and propagation of buzz-saw tones. The most recent analytical work on the full three-dimensional problem appears to have been by Sijtsma in 1995 [7]. Sijtsma presented a new non-linear analysis, capable of including the effect of acoustic lining, which predicted that buzz-saw noise will be significantly reduced by a passive acoustic liner in the aero-engine inlet duct. More recently CFD-based predictions of buzz-saw noise have been presented in an extensive report by Gliebe et al. [8]. (The terminology MPT—multiple pure tones—is used in Ref. [8].) Gliebe et al. conducted three-dimensional CFD simulations of several fan blade passages to investigate how modifications to the fan blades affected the MPT noise. They found that forward swept blades and blade sorting (changing the order of the blades around the fan disk) showed predicted MPT noise reductions. The effect of an acoustic liner on the buzz-saw/MPT noise was not considered in Ref. [8].

In this paper, predictions of buzz-saw noise in an acoustically lined aero-engine inlet duct are obtained by calculating the non-linear propagation of a sawtooth pressure signature. This approach is based on the plane two-dimensional model of the rotor-alone pressure field inside an aero-engine inlet duct proposed by researchers in the 1970s.

In 1970 Morfey and Fisher [9] calculated the non-linear attenuation of a regular sawtooth in terms of the "time of flight" T, where

$$T = a_0 t/\lambda = (z/D)K, \tag{1}$$

and

$$K = (B/\pi)\frac{M_{rel}^4}{\sqrt{M_{rel}^2 - 1}}(M_a\sqrt{M_{rel}^2 - 1} - M_t)^{-2}. \tag{2}$$

Note that a_0 is the undisturbed speed of sound (m s^{-1}), λ is the inter-shock spacing (m), B is the number of fan blades and D is the duct diameter (m). Eq. (1) relates the time of flight of a wave spiralling around a cylindrical duct in terms of the axial distance propagated (z).

Then for a regular sawtooth the shock strength p_s is given by

$$p_s(T) = P_0 s/(1 + ((\gamma + 1)/2\gamma)Ts), \tag{3}$$

where P_0 is the mean static pressure, γ is the adiabatic constant and $s = p_s(0)/P_0$ is the (non-dimensional) initial shock strength. Morfey and Fisher [9] derived Eq. (3) by using weak-shock theory.

Recently, Fisher et al. [10] used the sawtooth model in order to predict the noise from a supersonic ducted fan. Eq. (3) was used in Fisher et al. as a first approximation to describe the non-linear attenuation of a regular sawtooth in a hard-walled inlet duct. The non-linear propagation of an irregular sawtooth is calculable in the time domain. However, the main limitation of this approach is that there is no provision for the inclusion of the effect of the inlet duct wall on the attenuation of the waveform. In most modern aero-engines the inlet duct will have an acoustic lining covering a large portion of the available duct wall area. Fig. 2 is a sketch of a soft-walled (i.e., acoustically lined) cylindrical inlet duct (not to scale). The performance of an acoustic liner in an inlet duct will depend upon the mode number and frequency of the sound, and the speed of the oncoming flow. Fisher et al. recognized that in order to predict the effect of an acoustic liner on the rotor-alone tones, the problem should be transformed into the modal/frequency domain, enabling liner attenuation to be simply included in the model.

Following Fisher et al., in 2001 McAlpine and Fisher [11] considered the prediction of buzz-saw noise generated by an aero-engine by using two numerical simulation models. These models were identified by the acronyms time domain numerical solution (TDNS) and frequency domain numerical solution (FDNS). Both models calculate the non-linear propagation of an irregular sawtooth (representative of the pressure close to the inlet duct wall) in the time (TDNS) or frequency (FDNS) domain. In Ref. [11] the FDNS model was developed to be applicable with hard- or soft-walled inlet ducts. However in Ref. [11] results were confined to comparisons between the FDNS model and experimental data measured in a hard-walled inlet duct, (using data obtained by Rolls–Royce plc during the European Community research programme FANPAC). These comparisons suggested that the FDNS model may be used as a simple method to predict the rotor-alone tones in a hard-walled inlet duct.

In particular, by transforming the problem into the modal/frequency domain, the effect of cut-off in a hard-walled inlet duct at the low frequencies is included in the prediction. The effect of cut-off is not easily included in a time-domain model. Therefore in Ref. [11] the TDNS model was only used during the validation of FDNS. In theory the FDNS model may also be used with an acoustically lined inlet duct, provided that an estimate of the liner performance is known.

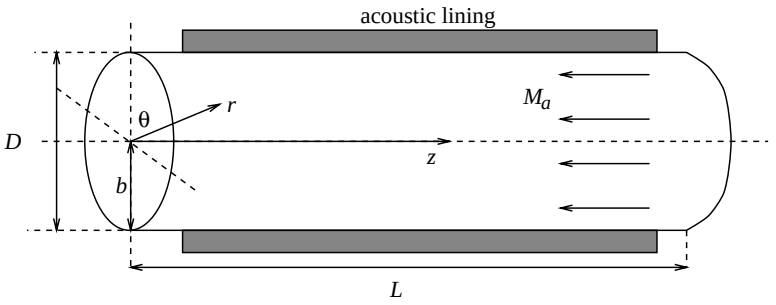

Fig. 2. Cylindrical inlet duct (not to scale).

The construction of an initial sawtooth to approximate the rotor-alone pressure field near the fan is described in Ref. [11]. This method relies on some prior knowledge of the amplitudes of the rotor-alone tones close to the fan plane. However the phases of these tones are not required, although without the phases it is not possible to construct a unique waveform. Therefore a sample of waveforms are constructed (each with a different set of initial phases for the rotor-alone tones) and the results from a series of FDNS simulations are averaged in order to generate a "mean" prediction. These simulations provide an estimate of the variation in the results due to small changes in the initial pressure signature (which may be thought of due to changes in the order of the blade stagger angle variations).

Experimentally, it is difficult to measure the "exact" sawtooth waveform near the fan because the required data sampling rate must be very high. In principle, if the location and amplitude of the shocks could be accurately "captured" by using a sufficiently high sampling rate, then the measured pressure signature close to the fan could be used as input to FDNS. This would permit a better comparison between experiment and theory because the initial phases of the rotor-alone tones would be known. In simplistic terms a measured sawtooth pressure signature may be viewed as a single "observation" for a fan. The numerical simulations may be viewed as predictions for a sample of "observations" for a fan, say undergoing a series of tests. This provides an estimate of the sensitivity of the tone levels to small changes in operating conditions (during each test). Thus the final "mean" FDNS prediction does not represent a precise attempt to predict the experimental data.

Both TDNS and FDNS are simple numerical prediction models. On a modern PC the run-times are about 60 s and 1 h, respectively. Therefore in order to generate a "mean" prediction, in practice, the FDNS model requires several hours computational run-time. This is predominantly due to the large number of EO harmonics to be calculated during each simulation. This number of harmonics largely determines the computational effort required, and a reduction in the number of harmonics to be calculated will improve the suitability of using FDNS as a simple prediction method.

In Ref. [11] the amount of numerical dissipation included in the FDNS model, in order to truncate the Fourier series expansion of the sawtooth waveform, was determined by comparison between the results from FDNS for a regular sawtooth, and the analytic theory (i.e., Eq. (3)). In Ref. [11] it was demonstrated that by calculating a large number of harmonics, up to frequencies of $100 \times$ BPF, then results obtained for frequencies up to about $10 \times$ BPF were comparable with regular sawtooth theory, provided there was sufficient dissipation included in the model. In this paper one demonstrates that less harmonics need to be calculated if the amount of dissipation is determined more precisely. The result is a more accurate simulation, with a run-time more comparable with TDNS.

The numerical dissipation largely dissipates energy at high frequencies (typically up to $100 \times$ BPF). In weak-shock theory it is implicitly assumed that the energy is dissipated by the shocks; this process is more efficient at high frequencies.

Section 2.1 briefly reviews the FDNS model developed in Ref. [11]. Then in Section 2.2 the non-linear propagation of a regular sawtooth with damping is considered. An analytic expression is derived (similar to Eq. (3)), with the rather idealized assumption that the damping is independent of mode number and frequency. It is shown that for a regular sawtooth the time or frequency domain approach will yield identical results provided that in the frequency domain *all* the modes are included in the calculation.

The effect of a realistic acoustic lining (with damping properties dependent on mode number and frequency of the sound, and the oncoming flow) may be included in FDNS. There will then be an additional source of dissipation in the numerical model. In theory the two sources of dissipation in FDNS are associated with significantly different frequency ranges. (An acoustic lining in an aero-engine inlet duct will usually be designed to provide maximum attenuation at frequencies close to the first few BPF harmonics.) In Section 2.2 a comparison between FDNS for a regular sawtooth (with damping), and analytic theory shows poor agreement. There is too much numerical dissipation in FDNS when the liner has reduced the tones to linear amplitudes.

In Section 2.3 the numerical dissipation required in the FDNS model with liner damping is determined more precisely. A method is outlined which improves the FDNS results (when compared with the analytic theory for a regular sawtooth), and requires significantly fewer harmonics to be calculated. This has the added benefit that the computational effort required is substantially reduced. In order to identify the changes to the FDNS model which are implemented in Section 2.3 in this paper, define FDNS(1) to denote the model in Ref. [11], and FDNS(2) to denote the model in this paper. (Note that the only difference between the two models is the numerical dissipation term.)

There is currently limited experimental data measured in acoustically lined inlet ducts for comparison with results from FDNS. In Section 3 experimental measurements of the liner insertion loss reported by Sarin and Rademaker in 1993 [12] are discussed. Ref. [12] details measurements of the liner insertion loss at the end of an inlet duct for the BPF tone. The insertion loss is a measure of the liner performance, although as will be seen it does not necessarily equal the predicted *linear* liner performance (see Section 2.2).

In Section 3 FDNS predictions of the rotor-alone tones in a hard-walled and acoustically lined inlet duct are compared. In particular the liner insertion loss for the BPF tone is predicted at two (supersonic) fan operating speeds. The experimental measurements and numerical results both suggest that at high fan speeds the liner insertion loss will be approximately zero. The results are discussed critically.

2. Theory

2.1. FDNS(1)

The FDNS model was described in McAlpine and Fisher [11], and only the necessary details are repeated in this paper. The non-linear propagation of an irregular sawtooth pressure signature is calculated by using

$$\partial p/\partial t + [(\gamma + 1)/2\rho_0 a_0]\, p\, \partial p/\partial x = 0, \tag{4}$$

where p is the deviation from P_0, ρ_0 is the mean density, and the spatial co-ordinate x (with velocity a_0) is the direction normal to the shock fronts (cf., Fig. 1). (In Ref. [13, pp. 648–656], Eq. (4)—the "simple wave equation"—is derived from the non-dissipative Euler equations by using the method of multiple scales.) On assuming the weak-shock approximation remains valid, then the propagation of a waveform including weak shocks may still be described by Eq. (4) (cf., Ref. [14, p. 176]).

On substituting the non-dimensional variables,

$$T = \frac{a_0 t}{\lambda}, \quad X = \frac{2\pi}{B}\frac{x}{\lambda} \quad \text{and} \quad P = \left(\frac{\gamma+1}{2\gamma}\right)\frac{p}{P_0} \tag{5}$$

into Eq. (4), the non-dimensional "simple wave equation" will be

$$\partial P/\partial T + (2\pi/B)P\,\partial P/\partial X = 0, \tag{6}$$

where B is the number of rotor blades (or equivalently the number of N-waves in the initial sawtooth).

The sawtooth is then expressed in terms of a complex Fourier series

$$P(X,T) = \sum_{m=-\infty}^{\infty} C_m(T)\mathrm{e}^{\mathrm{i}mX}, \tag{7}$$

where $C_{-m} = \tilde{C}_m$ ($\tilde{}$ denotes complex conjugate), and $C_0 \equiv 0$. The rotor-alone pressure field attached to a supersonic ducted rotor is thus expressed as a summation of Fourier modes; each mode m is steady in the rotor's frame of reference. The angular frequency ω and azimuthal wavenumber m of these modes are not independent. The ratio ω/m (circumferential phase velocity) is constant, and equals $2\pi\mathscr{F}$. Therefore the azimuthal wavenumber m is equivalent to the engine order (EO).

On substituting Eq. (7) into Eq. (6) the Fourier coefficients C_m may be calculated by integrating the set of coupled spectral differential equations:

$$\frac{\mathrm{d}C_m}{\mathrm{d}T} = -\frac{\mathrm{i}m\pi}{B}\left(\sum_{l=1}^{m-1} C_{m-l}C_l + 2\sum_{l=m+1}^{\infty} C_l\tilde{C}_{l-m}\right). \tag{8}$$

In FDNS(1) the Fourier series is truncated at the $m = N$th term, where $N \approx 100 \times B$. The accumulation of energy in the modes near $m = N$ is negated by the inclusion of numerical dissipation in the model. Burgers equation is the simplest model equation which includes non-linearity and dissipative effects. (The simple wave equation is simply Burgers equation without dissipation.) Therefore by using the non-dimensional Burgers equation

$$\partial P/\partial T + (2\pi/B)P\partial P/\partial X = (\varepsilon/B^2)\partial^2 P/\partial X^2, \tag{9}$$

Eq. (8) are approximated by

$$\frac{\mathrm{d}C_m}{\mathrm{d}T} = -\frac{\mathrm{i}m\pi}{B}\left(\sum_{l=1}^{m-1} C_{m-l}C_l + 2\sum_{l=m+1}^{N} C_l\tilde{C}_{l-m}\right) - \varepsilon\frac{m^2}{B^2}C_m. \tag{10}$$

Then a *linear* attenuation term $-\sigma(m)\,C_m$ may also be added to Eq. (10)

$$\frac{\mathrm{d}C_m}{\mathrm{d}T} = -\frac{\mathrm{i}m\pi}{B}\left(\sum_{l=1}^{m-1} C_{m-l}C_l + 2\sum_{l=m+1}^{N} C_l\tilde{C}_{l-m}\right) - \varepsilon\frac{m^2}{B^2}C_m - \sigma(m)C_m \tag{11}$$

to include (approximately) the effect of "cut-off" in a hard-walled, or liner damping in an acoustically lined inlet duct. In order to initiate this calculation one needs an initial set of Fourier coefficients $C_m(T_0)$ at an arbitrary position upstream of the fan ($T \approx T_0$). Subsequently Eq. (11) may be integrated numerically in order to obtain $C_m(T)$.

In Ref. [11] the FDNS(1) model was used to predict the rotor-alone tones in only a hard-walled inlet duct. The results were compared with experimental measurements, and there was reasonably close agreement between the predictions and data, particularly for the buzz-saw tones. In a hard-walled duct $\sigma \neq 0 \Leftrightarrow$ EO m is cut-off. Typically only several of the low-frequency buzz-saw EO modes will be cut-off. However in an acoustically lined inlet duct it is anticipated that $\sigma \neq 0$ for all m.

In FDNS(1) a relatively large number of EO harmonics were calculated ($N = 100 \times B$) in order to generate accurate results. With $N = 100 \times B$, provided there is sufficient dissipation at the high-frequency modes close to N, then results at considerably lower frequency mode numbers, approximately $1–10 \times B$, will not be adversely affected by truncating the Fourier series. However in order to reduce N then the numerical dissipation is required to be calculated more precisely.

2.2. Regular sawtooth with damping

Consider a regular sawtooth, and without loss of generality consider a single N-wave (i.e., $B = 1$, see Fig. 3). The Fourier coefficients C_m for an N-wave (with the shock positioned at $X = \pi$) are

$$C_m = (\mathrm{i}P_s/2\pi m)\cos m\pi, \tag{12}$$

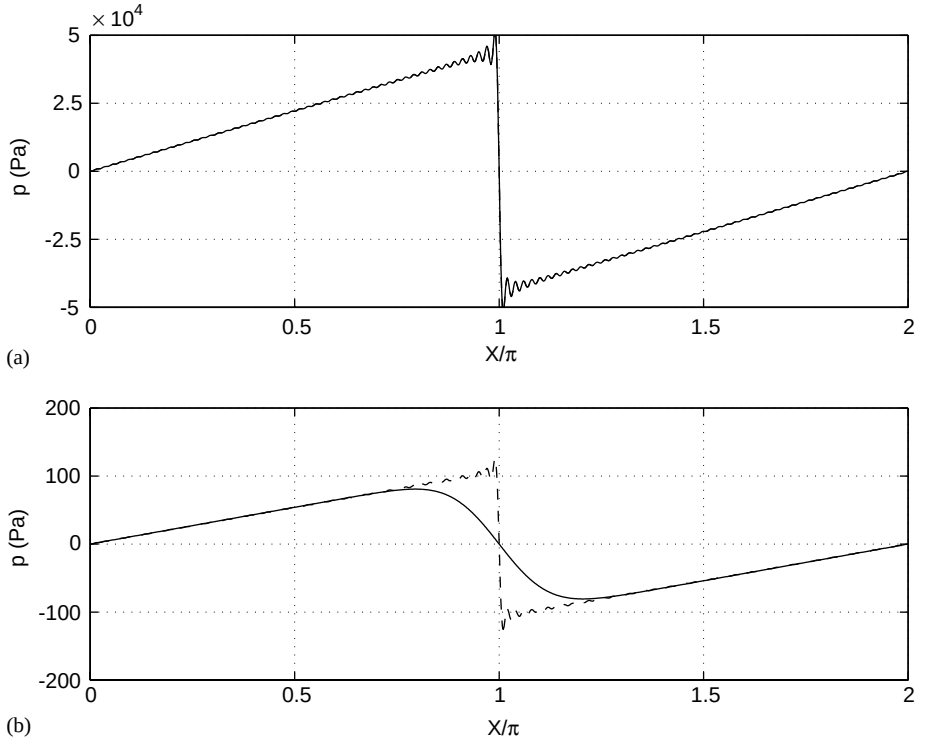

Fig. 3. Comparison between FDNS models (—, FDNS(1); and - - -, FDNS(2)) on propagating a regular sawtooth over the length of a typical inlet duct. Waveform (a) near the fan, and (b) near the end of the inlet duct.

where P_s is the (non-dimensional) shock strength, and it is now understood that m is equivalent to the BPF harmonic number. Now substitute Eq. (12) into Eq. (8) to obtain

$$\mathrm{d}P_s/\mathrm{d}T = -m^2 P_s^2 A(m), \tag{13}$$

where

$$A(m) = -\frac{1}{2}\sum_{l=1}^{m-1}\frac{1}{(m-l)l} + \sum_{l=m+1}^{\infty}\frac{1}{l(l-m)}. \tag{14}$$

The infinite summation in Eq. (14) is convergent, and it is straightforward to show that

$$m^2 A(m) = 1. \tag{15}$$

Therefore Eq. (13) reduces to

$$\mathrm{d}P_s/\mathrm{d}T = -P_s^2, \tag{16}$$

(now independent of m) which may be integrated to obtain

$$p_s(T) = P_0 s/(1 + ((\gamma+1)/2\gamma)Ts), \quad s = p_s(0)/P_0. \tag{17}$$

Eq. (17) describes the non-linear attenuation of a regular sawtooth, and was originally calculated by Morfey and Fisher [9] by using weak-shock theory.

Now consider the non-linear propagation of a regular sawtooth through an attenuating medium with absorption properties independent of mode number and frequency. Then the BPF harmonics of the waveform will all be attenuated at the same rate, and the profile will remain a regular sawtooth. Eq. (6) is modified by the inclusion of a linear damping term

$$\partial P/\partial T + (2\pi/B)P\partial P/\partial X = -\sigma_B P, \tag{18}$$

where σ_B is a real constant, prescribing the attenuation rate of *all* the BPF harmonics in the sawtooth. Now on substituting Eq. (7) into Eq. (18)

$$\frac{\mathrm{d}C_m}{\mathrm{d}T} = -\frac{\mathrm{i}m\pi}{B}\left(\sum_{l=1}^{m-1} C_{m-l}C_l + 2\sum_{l=m+1}^{\infty} C_l\tilde{C}_{l-m}\right) - \sigma_B C_m, \tag{19}$$

and then substituting Eq. (12) into Eq. (19)

$$\mathrm{d}P_s/\mathrm{d}T = -P_s^2 - \sigma_B P_s. \tag{20}$$

Eq. (20) may also be integrated to obtain

$$p_s(T) = P_0 s\mathrm{e}^{-\sigma_B T}/(1 + ((\gamma+1)/2\gamma)Ts([1-\mathrm{e}^{-\sigma_B T}]/\sigma_B T)). \tag{21}$$

Eq. (21) describes the non-linear attenuation of a regular sawtooth propagating through a fluid with absorption independent of mode number and frequency. Eq. (21) was originally derived by Fisher et al. [10] as a first approximation to describe the non-linear attenuation of a regular sawtooth in an acoustically lined inlet duct.

In the limit as $\sigma_B \to 0$, Eqs. (17) and (21) are equivalent. Further, Eqs. (17) and (21) may be approximated by

$$p_s(T) \approx \frac{P_0}{((\gamma+1)/2\gamma)T} \quad \text{and} \quad p_s(T) \approx \frac{P_0}{((\gamma+1)/2\gamma)T}\mathrm{e}^{-\sigma_B T}\sigma_B T, \tag{22}$$

when $Ts \gg 1$ (and also assuming that $\sigma_B \ll s$). It is well known that for a regular sawtooth $p^2_{r.m.s.} = p^2_s/12$, and the overall sound pressure level (OASPL) is given by

$$\text{OASPL} = 10\log_{10}(p^2_{r.m.s.}/P^2_{ref}) = 10\log_{10}(\tfrac{1}{12}p^2_s/P^2_{ref}). \tag{23}$$

Also the SPL of the BPF tone for a regular sawtooth is given approximately by

$$\text{SPL} \approx \text{OASPL} - 2.16 \text{ dB}. \tag{24}$$

Therefore the SPL of the BPF tone in a hard-walled and acoustically lined duct will be given approximately by

Hard-walled:

$$\text{SPL} \approx 182.34 - 20\log_{10} T, \tag{25}$$

Lined:

$$\text{SPL} \approx 182.34 - 20\log_{10} T - 20\sigma_B T\log_{10} e + 20\log_{10}\sigma_B T. \tag{26}$$

Define the liner insertion loss to be the difference between the SPL by the end of the inlet duct when the duct wall is hard and acoustically lined. From Eqs. (25) and (26) the predicted liner insertion loss for a regular sawtooth will be

$$20\sigma_B T_L\log_{10} e - 20\log_{10}\sigma_B T_L, \tag{27}$$

where $T = T_L$ by the end of the inlet duct. Note that $20\sigma_B T_L\log_{10} e$ is the predicted *linear* liner insertion loss, and $20\log_{10}\sigma_B T_L$ is a non-linear correction. Therefore prediction of the SPL at the end of an acoustically lined inlet duct may not necessarily be determined by simply subtracting the *linear* liner performance from the measured SPL in a hard-walled duct. Overall in the lined duct there will be less non-linear attenuation because the tones will decay more rapidly to linear amplitudes because of the presence of the acoustic lining.

Fig. 4 shows a comparison between FDNS(1) results for a regular sawtooth with damping, and the analytic theory (i.e., Eq. (21)). (An arbitrary value for σ_B is used in this example.) Results are shown for 1, 5 and 10 × BPF. The comparison between the results is good at BPF, but poor at 5 and 10 × BPF. With the inclusion of damping the BPF harmonics are rapidly attenuated to linear amplitudes. In practice when $P \ll 1$ (i.e., linear acoustics) Eq. (11) should reduce to

$$\mathrm{d}C_m/\mathrm{d}T = -\sigma(m)C_m. \tag{28}$$

However Eq. (11) reduces to

$$\mathrm{d}C_m/\mathrm{d}T = -(\varepsilon m^2/B^2 + \sigma(m))C_m, \tag{29}$$

and there will remain too much dissipation in the FDNS(1) model. The inclusion of damping increases the attenuation of the BPF harmonics (compared with a hard-walled duct when $\sigma \equiv 0$ for all the BPF harmonics) and the excess dissipation in Eq. (29) is likely to adversely affect the results. In FDNS(1) the numerical dissipation rate ε is a constant. In a hard-walled inlet duct (of typical length) this assumption is reasonable because it is unlikely that the harmonics will be attenuated to linear amplitudes.

However in an acoustically lined inlet duct the harmonics are more likely to be attenuated to linear amplitudes, and it will be necessary to reduce ε accordingly. Therefore in Section 2.3 the numerical dissipation rate ε is determined more precisely by reducing ε following the decay of a

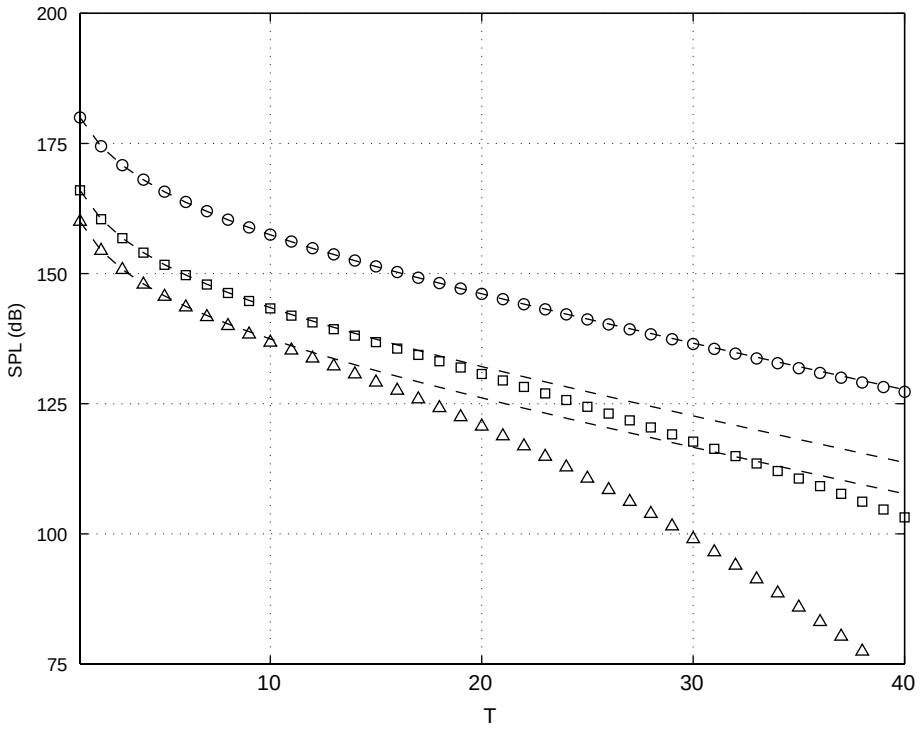

Fig. 4. Comparison between FDNS(1) results for a regular sawtooth (with damping), and the analytic theory: - - -, regular sawtooth; ○, 1 × BPF; □, 5 × BPF and △, 10 × BPF.

regular sawtooth waveform when $T \gg 1$. This change appears necessary when calculating the rotor-alone tones in an acoustically lined inlet duct.

2.3. FDNS(2)

Once again consider a regular sawtooth (i.e., a single N-wave, $B = 1$ and m is the BPF harmonic number) and now re-arrange Eqs. (19)

$$\frac{\mathrm{d}C_m}{\mathrm{d}T} = -\frac{\mathrm{i}m\pi}{B}\left(\sum_{l=1}^{m-1} C_{m-l}C_l + 2\sum_{l=m+1}^{N} C_l\tilde{C}_{l-m}\right) - \frac{\mathrm{i}m\pi}{B}\left(2\sum_{l=N+1}^{\infty} C_l\tilde{C}_{l-m}\right) - \sigma_B C_m. \tag{30}$$

In 1996 Pishchal'nikov et al. [15] proposed a novel method to reduce the number of Fourier harmonics necessary to be computed for waveforms with a single shock. Essentially they derived an analytic expression for the term in Eq. (30) containing the infinite summation; the amplitude of the shock P_s was determined by using a matching condition at $m = N$. Then Eqs. (30) may be numerically integrated with the number of harmonics N reduced to about 10 (for a single shock). They did not discuss an extension to this method for waveforms containing more than one shock.

In this paper a similar method to that proposed in Ref. [15] is used in order to reduce the number of harmonics N to be calculated in FDNS(2). On substituting Eq. (12) into Eq. (30)

$$\frac{\mathrm{d}P_s}{\mathrm{d}T} = -m^2 A(m,N)P_s^2 - m^2\left\{\sum_{l=N+1}^{\infty}\frac{1}{l(l-m)}\right\}P_s^2 - \sigma_B P_s, \tag{31}$$

where

$$A(m,N) = -\frac{1}{2}\sum_{l=1}^{m-1}\frac{1}{(m-l)l} + \sum_{l=m+1}^{N}\frac{1}{l(l-m)}. \tag{32}$$

Following Ref. [15], Eq. (31) is equivalent to

$$\frac{\mathrm{d}P_s}{\mathrm{d}T} = -m^2 A(m,N)P_s^2 - m\left\{\sum_{l=N-m+1}^{N}\frac{1}{l}\right\}P_s^2 - \sigma_B P_s. \tag{33}$$

However in FDNS(1), on substituting Eq. (12) into Eq. (11)

$$\mathrm{d}P_s/\mathrm{d}T = -m^2 A(m,N)P_s^2 - \varepsilon m^2 P_s - \sigma_B P_s, \tag{34}$$

with ε a constant. Compare Eqs. (33) and (34), and in FDNS(2) redefine ε such that

$$\varepsilon = \bar{\varepsilon}(m,N)P_s(T) = \frac{1}{m}\left\{\sum_{l=N-m+1}^{N}\frac{1}{l}\right\}P_s(T), \tag{35}$$

with non-dimensional shock strength P_s given by

$$P_s(T) = \frac{\mathrm{e}^{-\sigma_B T}}{(\frac{2\gamma}{\gamma+1})\frac{1}{s} + ([1-\mathrm{e}^{-\sigma_B T}]/\sigma_B)} \tag{36}$$

from Eq. (21). The dissipation rate ε is now a function of the BPF harmonic number m, the number of terms N in the Fourier series, and the amplitude of the shock P_s.

It is straightforward to extend this definition of ε (35) to be used in FDNS(2) for an irregular sawtooth. Eq. (35) defines $\varepsilon = \bar{\varepsilon}(m,N)P_s(T)$ for a regular sawtooth with m the BPF harmonic mode number. For an irregular sawtooth m is now the EO mode number. By using linear interpolation between successive BPF harmonic mode numbers, a linear piece-wise continuous function $\bar{\varepsilon}(m,N)$ may be constructed which is valid for all EO mode numbers m. Higher order interpolation is not required.

P_s (the non-dimensional shock strength) has been calculated for a regular sawtooth assuming that the attenuation rate σ_B is a constant. Therefore all the BPF harmonics are attenuated at the same rate, maintaining a regular sawtooth waveform. For an irregular sawtooth Eq. (36) will remain a valid expression giving the reduction in ε with increasing T provided that the assumption that all the BPF harmonics are damped at the same rate is a reasonable approximation. This will depend on the nature of the acoustic lining in the inlet duct.

An alternative estimate for P_s may be calculated from the overall SPL. At each step in the Runge–Kutta integration the OASPL may be calculated by summing up the energy in all the

Fourier harmonics. For a regular sawtooth, from Eqs. (23) and (5)

$$\mathrm{OASPL} = 10\log_{10}((2\gamma P_0)^2/12(\gamma+1)^2 P_{ref}^2) + 10\log_{10} P_s^2. \tag{37}$$

By rearranging Eq. (37) P_s may be determined from the OASPL.

For an irregular sawtooth propagating in an acoustically-lined inlet duct the notion of a single shock strength characterizing the waveform is no longer valid assuming that in practice the liner's performance will be frequency dependent. In this case the factor $P_s(T)$ multiplied by $\bar{\varepsilon}(m,N)$ in Eq. (35) is best determined from the OASPL at each step in the numerical integration. (This will slightly increase the computational effort because the OASPL has to be calculated at each step in the integration.) Now $P_s(T)$ is a parameter determined by the overall energy in the waveform. As this energy is dissipated by the acoustic lining the numerical dissipation in FDNS will decrease proportional to the overall energy remaining in the waveform. The FDNS(2) results shown in Section 3 are calculated with P_s determined by the OASPL.

In summary, in FDNS(2) the coupled spectral differential equations are now

$$\frac{\mathrm{d}C_m}{\mathrm{d}T} = -\frac{\mathrm{i}m\pi}{B}\left(\sum_{l=1}^{m-1} C_{m-l}C_l + 2\sum_{l=m+1}^{N} C_l\tilde{C}_{l-m}\right) - \bar{\varepsilon}(m,N)P_s(T)\frac{m^2}{B^2}C_m - \sigma(m)C_m, \tag{38}$$

where $\sigma(m)$ simulates the effect of liner damping. The linear attenuation rate $\sigma(m)$ is dependent upon mode number m (or frequency), and is calculated by setting

$$\sigma(m) = \mathrm{Re}\{\mathrm{i}k_z D/K\} = -k_{zi}D/K, \tag{39}$$

where $k_z = k_{zr} + \mathrm{i}k_{zi}$ is the axial wavenumber for the least attenuated radial duct mode with azimuthal mode number m, and K is defined by Eq. (2). The calculation of $\sigma(m)$ for a locally reacting acoustic lining is described in Ref. [11]; brief details are included in this paper in Appendix A.

Now in Section 2.4, it is shown that for an irregular sawtooth this modification is sufficient to generate accurate results, with N reduced from $100 \times B$ to $10 \times B$. This leads to a large reduction in the run-time.

2.4. Validation of FDNS(2)

Firstly, consider a regular sawtooth with damping, and compare the respective results from FDNS(1) and FDNS(2) with the analytic theory (i.e., Eq. (21)). Fig. 3 shows an N-wave calculated by using FDNS(1) and FDNS(2). The initial waveforms in Fig. 3(a) are propagated over the length of a typical inlet duct. In theory the waveforms are predicted to maintain their N-wave shape because all the harmonics are attenuated at the same rate. By the end of the inlet duct (see Fig. 3(b)) the waveform calculated by FDNS(1) no longer contains a shock, because there is too much dissipation in the model. However by using FDNS(2) the N-wave maintains its shape. (Note that in Fig. 3(a) and (b) Gibbs phenomenon is clearly visible on the high- and low-pressure sides of the shock.)

Fig. 5 shows a comparison between FDNS(2) results for a regular sawtooth with damping, and the analytic theory, using the same arbitrary value of σ_B used in the previous example shown in

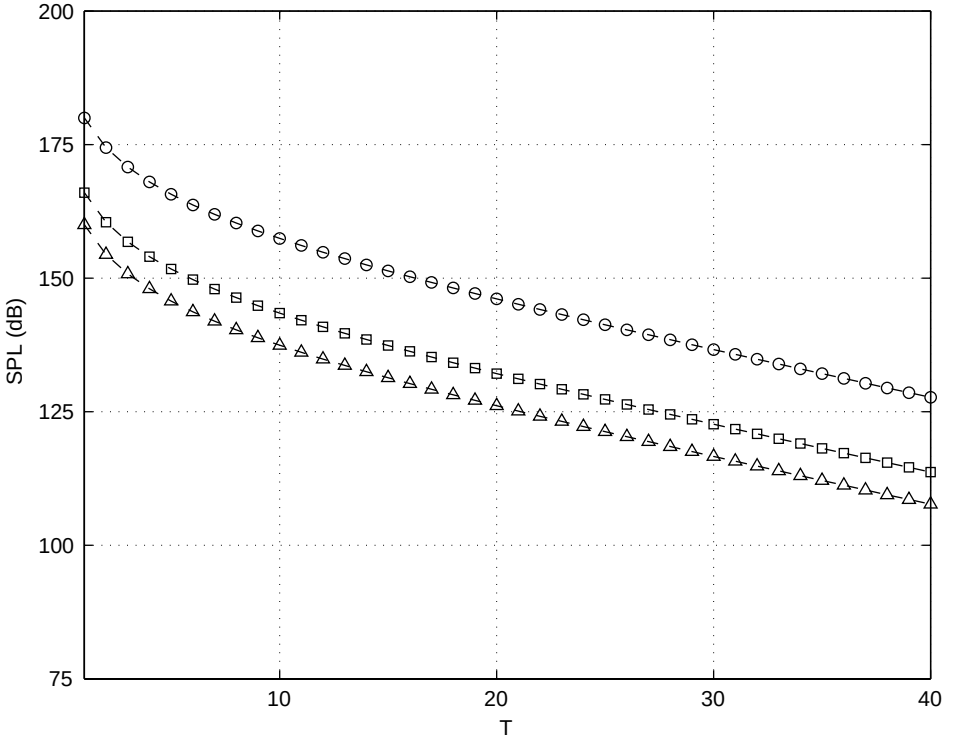

Fig. 5. Comparison between FDNS(2) results for a regular sawtooth (with damping), and the analytic theory: - - -, regular sawtooth; ○, 1 × BPF; □, 5 × BPF and △, 10 × BPF.

Fig. 4. Compare the results obtained by using FDNS(1) with $N = 100 \times B$, and FDNS(2) with $N = 10 \times B$, in Figs. 4 and 5, respectively. There is now exact agreement between the FDNS(2) results and regular sawtooth theory. (The numerical dissipation term used in FDNS(2) was derived by using the regular sawtooth theory, and therefore the results are expected to show precise agreement with this theory.)

Secondly, consider a "typical" irregular sawtooth waveform constructed close to a ducted fan. This example uses the identical irregular sawtooth constructed in Ref. [11] (Section 2.3, Figs. 11 and 12) when validating FDNS(1) with the time-domain model TDNS. Figs. 6 and 7 show a comparison between results from FDNS(1) and FDNS(2) (again with $N = 100 \times B$ and $10 \times B$, respectively). Fig. 6 shows the first four BPF harmonics plotted against T, (i.e., plotting the attenuation over the length of a typical inlet duct). Fig. 7 compares the EO frequency spectrum at two axial stations in the duct located (a) near the fan, and (b) near the end of the inlet duct. In the examples in this paper there is clearly exact agreement up to frequencies of $4 \times$ BPF. Therefore these results (Figs. 6 and 7) together with Figs. 11 and 12 in Ref. [11] demonstrate the equivalence of results obtained by using either TDNS, FDNS(1) or FDNS(2).

The run-time (over a typical duct length) for TDNS and FDNS(1) is about 60 s and 1 h, respectively. With the reduction in the number of harmonics to be calculated in FDNS(2), the run-time for FDNS(2) is now also about 60 s, comparable with the time-domain model. However

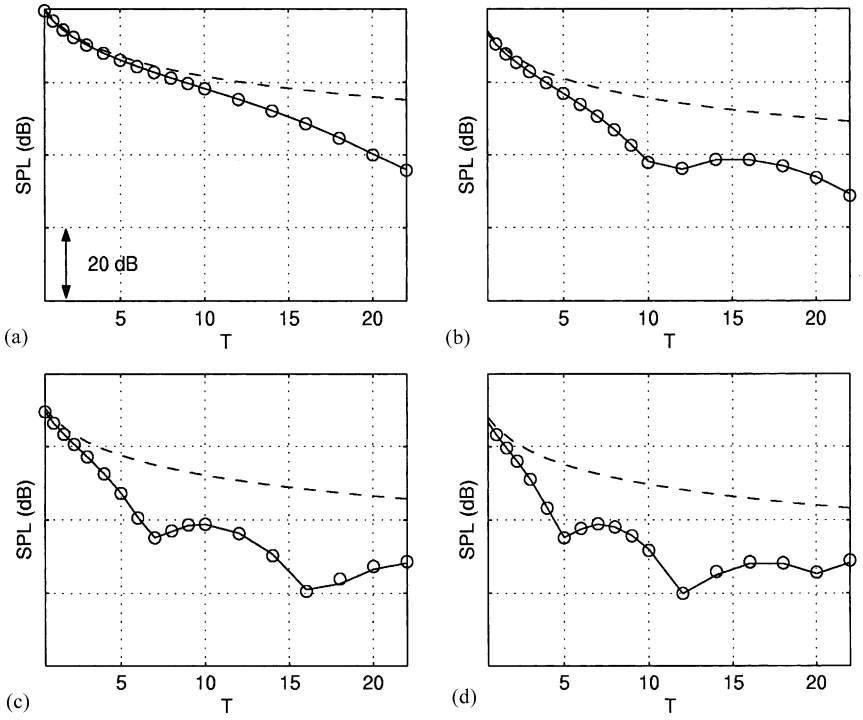

Fig. 6. Comparison between FDNS models (—, FDNS(1); and ○, FDNS(2)) on propagating an irregular sawtooth over the length of a typical inlet duct. Note - - - denotes the attenuation of the BPF harmonics for a regular sawtooth: (a) 1 × BPF; (b) 2 × BPF; (c) 3 × BPF and (d) 4 × BPF.

FDNS includes the effect of cut-off in a hard-walled duct and an acoustic lining in a soft-walled duct.

3. Results

In McAlpine and Fisher [11] experimental data obtained by Rolls–Royce plc during the FANPAC research programme was compared against simulation results from FDNS. The measured data was all obtained in a hard-walled inlet duct. In Ref. [11] results from FDNS compared reasonably well with measured EO frequency spectra in the FANPAC hard-walled inlet duct (at two axial stations located at $z/D = 0.25$ and 0.5). While it is hoped in the future to present detailed comparisons with measurement from lined inlet ducts, in this paper the capability of FDNS is demonstrated by considering a "model" fan and inlet duct, with a locally reacting perforate acoustic lining (known as a SDOF—single degree of freedom—liner).

In 1993 Sarin and Rademaker [12] reported in-flight measurements obtained in an untreated (hard-walled) and acoustically lined inlet duct of the Rolls–Royce Tay 650 engine, of a Fokker 100 aircraft. Modal measurements were obtained upstream of the acoustic lining by using a microphone array positioned around the circumference of the engine intake lip. The SPL of the

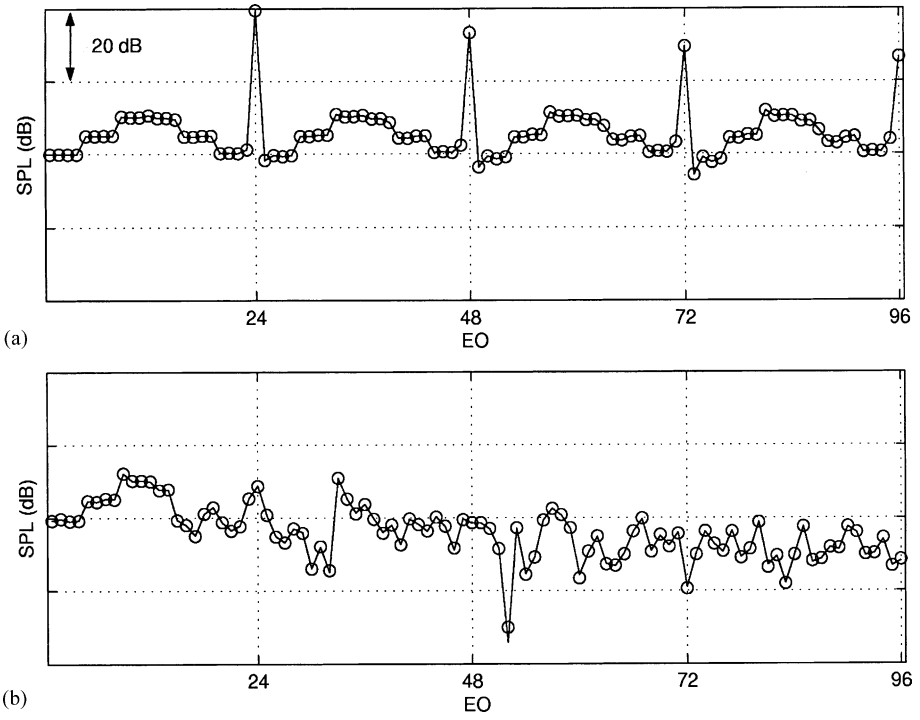

Fig. 7. Comparison between FDNS models (—, FDNS(1); and ○, FDNS(2)) on propagating an irregular sawtooth over the length of a typical inlet duct. EO frequency spectrum (a) near the fan, and (b) near the end of the inlet duct.

BPF tone was measured at the engine intake lip, with and without the acoustic treatment, over a range of engine speeds. The results were shown in Ref. [12, Fig. 8, p. 7], and are recreated in Fig. 8 in this paper. This illustrates the measured liner insertion loss as a function of the engine fan speed (nominal load—NL). (Note that the NL specified in Ref. [12] was corrected for atmospheric conditions at the flight altitude.)

In Fig. 8 the measured level in the hard-walled inlet duct increases rapidly above $\approx 60\%$ NL. This is close to when the fan tip speed becomes sonic. Between 65% NL and 80% NL the measured liner insertion loss is between 10 and 20 dB. However above 80% NL the liner insertion loss is approximately zero. In Ref. [12] it was also reported that buzz-saw noise became important at fan speeds above 76% NL in the hard-walled inlet. However with the treated configuration the dominant tones were the BPF harmonics. It was suggested that the decrease in the SPL of the BPF tone measured in the hard-walled inlet duct at high speeds may be caused by the occurrence of buzz-saw noise.

A direct comparison between these experimental measurements and FDNS results is not possible because additional information not in Ref. [12] is required. Measurements in Ref. [12] were obtained under flight conditions. Thus the Mach flight number rather than the inlet duct Mach number (M_a) is known. Therefore at each engine operating speed (NL) only M_t, and not M_a, is accurately deducible from the information detailed in Ref. [12].

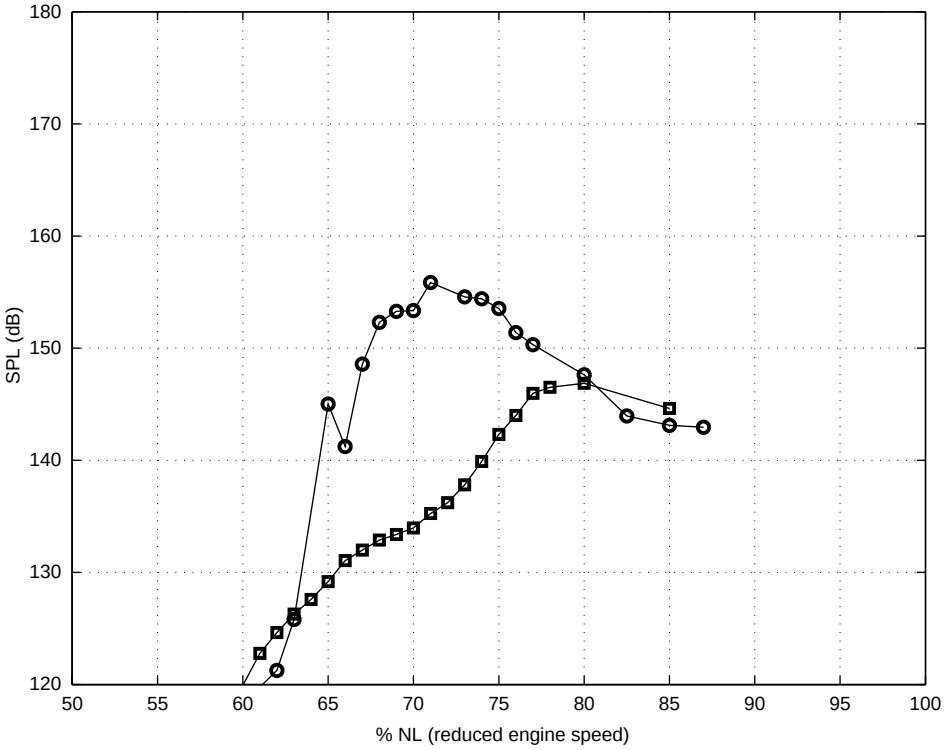

Fig. 8. BPF tone measured at the engine intake lip, with (□) and without (○) acoustic lining, in the inlet duct of the Rolls–Royce Tay 650 engine (after Sarin and Rademaker [12, Fig. 8, p. 7]).

Hence results in this paper are presented based on flow speeds with relative Mach number M_{rel} approximately 1.2 and 1.4. M_{rel} is chosen to be the parameter to identify the different FDNS predictions because in the authors' experience $M_{rel} \approx 1.2$ corresponds to when buzz-saw noise first starts to become significant. Sarin and Rademaker note that buzz-saw noise is significant for speeds above 76% NL. Therefore it is likely that the moderate supersonic operating speed $M_{rel} \approx 1.2$ corresponds approximately to a NL between 70% and 80%; the higher supersonic operating speed $M_{rel} \approx 1.4$ is likely to correspond to a NL above 80%.

FDNS results are calculated for a ''model' 'fan with 22 fan blades, diameter $D = 1.16$ m and design r.p.m. = 8393. The acoustic lining extends over a length equivalent to $0.45D$, has porosity $\rho = 5.5\%$ and depth $h = 0.028$ m. The impedance of this lining is calculated by using Eqs. (A.6) and (A.7) (cf., Appendix A). The specification for this ''model'' fan, inlet and lining is based on the description in Ref. [12] of the Rolls–Royce Tay 650 engine.

Measurements of the EO frequency spectrum close to the fan are not available from Ref. [12] to use for the initial conditions in the FDNS simulations. Therefore the initial sawtooth waveform (approximating the rotor-alone pressure field at the fan face) is constructed by inferring from Ref. [12] that close to the fan the BPF tone level is ≈ 170 dB, and the buzz-saw tone level is approximately 20–30 dB less than BPF. It is assumed that the highest levels in the buzz-saw tones occur at frequencies close to $\frac{1}{2} \times$ BPF. (See Ref. [11] for examples of EO frequency spectra

measured close to the fan face in an inlet duct. The FDNS set-up procedure is also outlined in Ref. [11], and not repeated in this paper.) It is assumed that the initial waveform located close to the fan face will be the same with or without an acoustic liner in the inlet duct. The non-linear propagation of this waveform ensures that the accuracy of this initial estimate of the irregular sawtooth will have less effect on the subsequent results obtained at the end of the inlet duct, compared with a linear propagation model.

The predicted *linear* liner performance at $M_{rel} \approx 1.2$ and 1.4 is shown in Fig. 9. The modal attenuation rates predict *linear* attenuation for a length of lining $= 0.45D$ (i.e. the length of acoustical lining in the inlet duct). At each speed the peak attenuation is at a frequency less than BPF. At $M_{rel} \approx 1.2$ the attenuation at BPF (EO = 22) is about four times greater than at $M_{rel} \approx 1.4$. There is also a broader band of EOs predicted to be well-attenuated at the lower speed. It is straightforward to calculate that at $M_{rel} \approx 1.2$ in a hard-walled duct EO 1–4 are cut-off, whereas when $M_{rel} \approx 1.4$ only EO 1 is cut-off.

FDNS predictions of the attenuation of the BPF tone in the inlet duct, and the EO frequency spectrum near the intake lip (up to $4 \times$ BPF), are shown in Figs. 10 and 11, respectively.

In Fig. 10 the attenuation of the BPF tone against distance upstream in the inlet duct is compared at each speed with the comparable attenuation of a regular sawtooth waveform (by using Eqs. (3) and (21)). This estimates the attenuation of the tone in the absence of any buzz-saw energy.

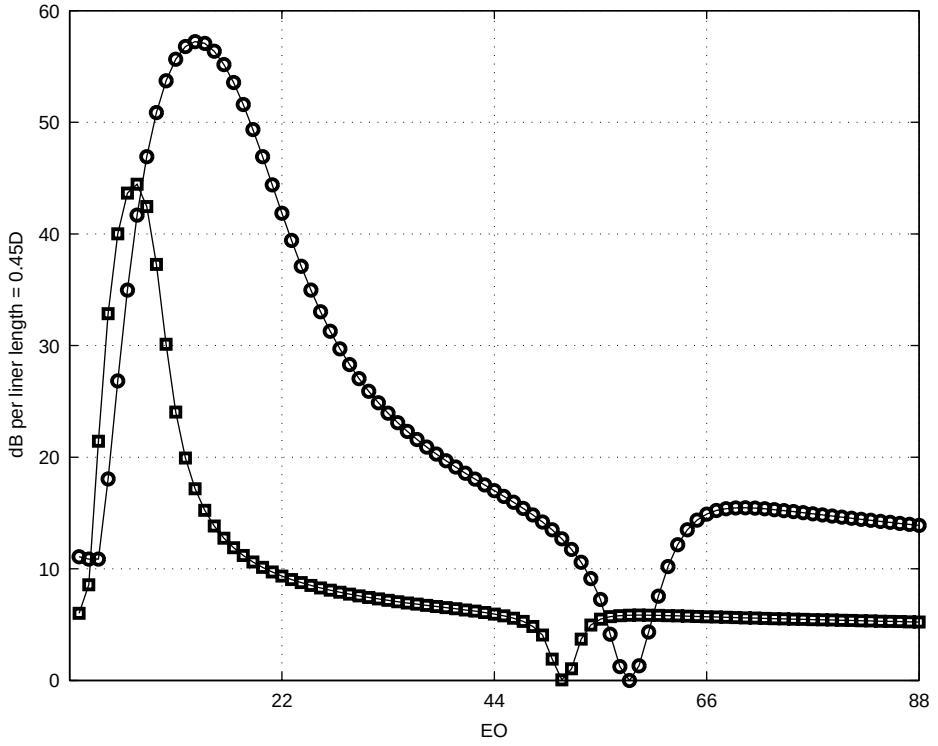

Fig. 9. Predicted *linear* liner performance at $M_{rel} \approx 1.2$ (○) and $M_{rel} \approx 1.4$ (□). Inlet and fan based on specification outlined in Ref. [12].

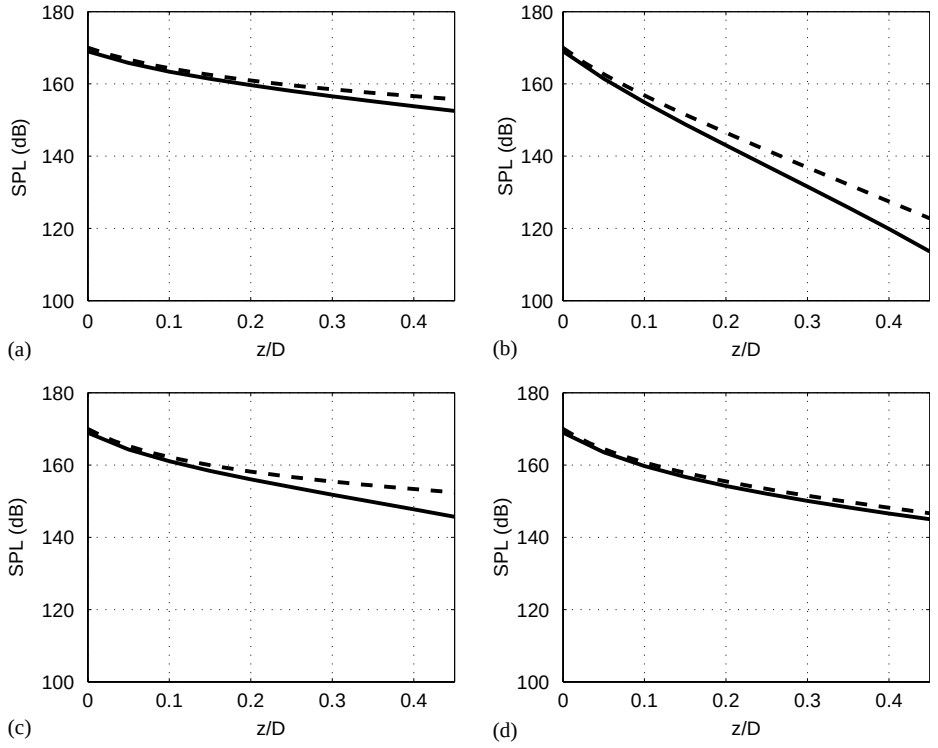

Fig. 10. Predicted attenuation of BPF tone (calculated using FDNS(2)), - - - regular sawtooth and — irregular sawtooth: (a) hard-walled inlet $M_{rel} \approx 1.2$; (b) lined inlet $M_{rel} \approx 1.2$; (c) hard-walled inlet $M_{rel} \approx 1.4$ and (d) lined inlet $M_{rel} \approx 1.4$. Inlet and fan based on specification outlined in Ref. [12].

In the hard-walled inlet duct the difference between the FDNS and regular sawtooth predictions of the attenuation of the BPF tone is slightly greater at the higher speed (compare Fig. 10(a) and (c)). The presence of high-amplitude buzz-saw tones will facilitate non-linear attenuation of the BPF tone through sum and difference non-linear spectral interactions between *all* the EO harmonics (compared with a regular sawtooth in which all the energy and hence non-linear interactions are confined to the BPF harmonics). At higher speeds less of the low-frequency EO buzz-saw modes will be cut-off, enabling the likelihood of more attenuation of the BPF tone. Also the waveform will be swept more times around the inlet at the higher speeds leading to a longer "time of flight" T in the duct. In a hard-walled inlet duct the level of the BPF tone at the end of the duct will typically become slightly lower with increasing M_{rel} (or equivalently increasing NL). However there is likely to be more buzz-saw noise at the higher speeds.

Comparing the level of the BPF tone at the end of the inlet duct at the two supersonic speeds; at $M_{rel} \approx 1.4$ the BPF tone is about 7 dB less compared with the corresponding level when $M_{rel} \approx 1.2$. Note that Sarin and Rademaker measure a reduction in the level of the BPF tone of slightly over 10 dB in the hard-walled inlet duct when the operating speed is increased from about 70% NL to 85% NL (see Fig. 8).

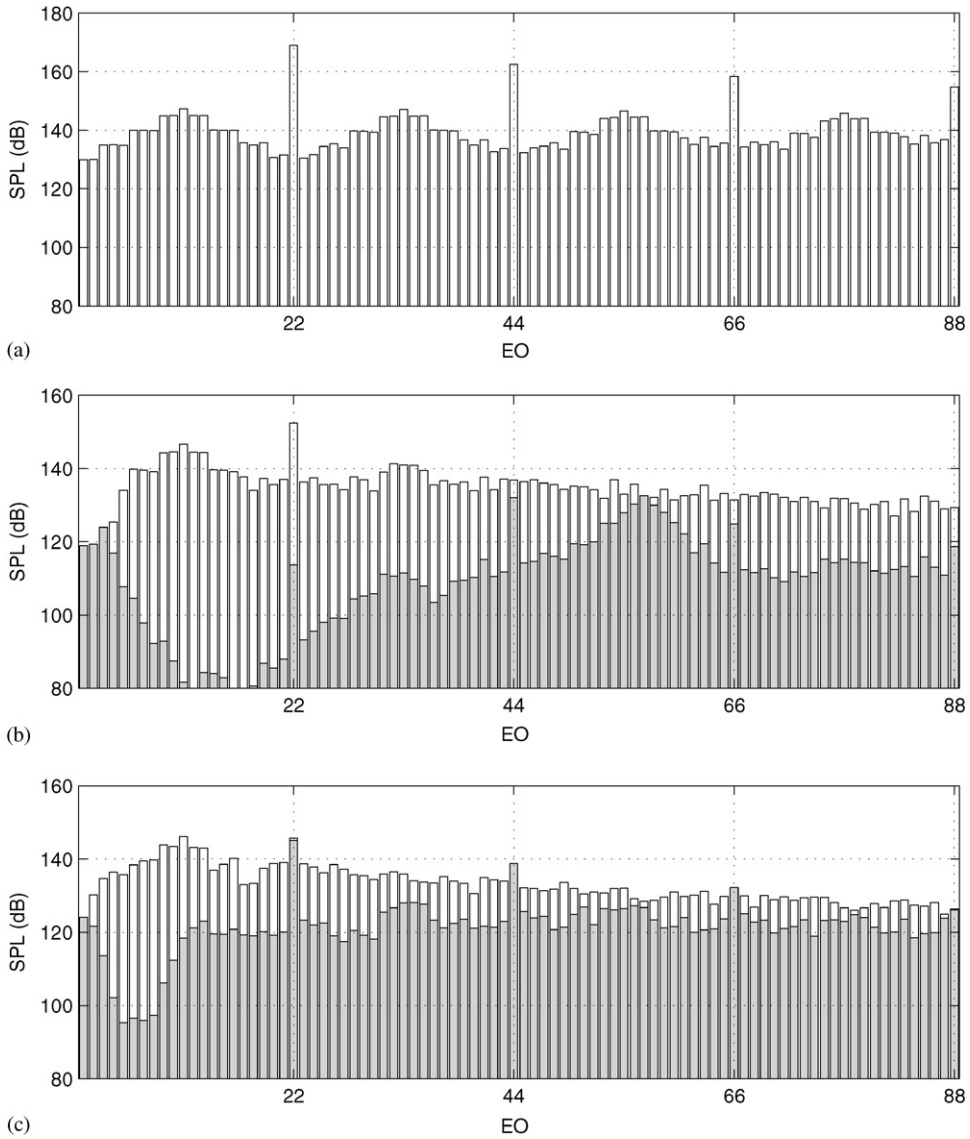

Fig. 11. Predicted EO frequency spectra (up to 4 × BPF): (a) estimated initial EO frequency spectrum close to the fan face, (b) predicted EO frequency spectrum near the end of the inlet duct for $M_{rel} \approx 1.2$, and, (c) predicted EO frequency spectrum near the end of the inlet duct for $M_{rel} \approx 1.4$. Predictions of EO frequency spectrum near the end of the inlet duct in (b) and (c) are shown with a hard-walled inlet (white bars) and lined inlet (grey bars). Inlet and fan based on specification outlined in Ref. [12].

In the lined inlet the BPF tone is well-attenuated at $M_{rel} \approx 1.2$ compared with the higher speed (compare Fig. 10(b) and (d)). At $M_{rel} \approx 1.2$ there is predicted to be about 40 dB of *linear* attenuation (cf., Fig. 9). The overall attenuation is predicted to be about 55 dB—the additional 15 dB is due to non-linearity. However at $M_{rel} \approx 1.4$ there is only predicted to be about 10 dB of

linear attenuation, and the overall attenuation is now predicted to be about 25 dB. The attenuation of the BPF tone in the lined inlet (at this higher speed) more closely resembles the predicted attenuation in the hard-walled inlet duct (compare Fig. 10(c) and (d)).

In the lined duct at $M_{rel} \approx 1.4$ the lining will still slightly attenuate the BPF tone; however, at this speed the low-frequency EO buzz-saw tones are well-attenuated by the lining, reducing any non-linear interactions involving these EOs. In the hard-walled inlet duct the BPF tone's attenuation is facilitated by these high-amplitude buzz-saw tones—therefore at $M_{rel} \approx 1.4$ the overall difference in the BPF tone level between the hard-walled and acoustically lined inlet duct, at the engine intake lip, is approximately zero.

The non-linear attenuation predicted by the analytic theory for a regular sawtooth (Eqs. (3) and (21)) appears to be a reasonable first approximation in order to determine the attenuation of the BPF tone in an engine inlet duct. However this theory (with an acoustic liner) assumes that all the BPF harmonics will be attenuated at the same rate. Therefore with an acoustically lined duct this theory is only likely to be applicable in order to predict the BPF tone, because in general the liner performance at the higher BPF harmonics will change significantly compared with at BPF. (Note that σ_B is set equal to $\sigma(B)$ in Eq. (21).)

These predictions (consistent with the observations in Ref. [12]) show that at moderate sonic operating speeds, when there is good liner performance, there will be a significant liner insertion loss at BPF. However this insertion loss is not maintained at higher speeds because of the loss of liner performance at most EOs, apart from (some of) the low-frequency EO buzz-saw tones. Although the liner insertion loss at BPF may lessen with increasing speed, the buzz-saw noise is likely to be reduced at all fan speeds with this type of SDOF perforate liner.

In Fig. 11 predicted EO frequency spectra (near the intake lip) are compared between the hard-walled and acoustically lined inlet duct, at both $M_{rel} \approx 1.2$ and 1.4. Fig. 11(a) shows the estimated EO frequency spectrum used in each simulation to represent the pressure field at the fan face. The benefit of the lining is most clearly apparent at $M_{rel} \approx 1.2$. In this model simulation the only tones which do not suffer any sizeable attenuation are the low-frequency EOs 1–4 (which are cut-off), and at EOs close to the anti-resonance frequency. The BPF harmonics remain clearly visible tones in the EO frequency spectrum.

However the benefit of the lining is predicted to be considerably less at $M_{rel} \approx 1.4$. Sizeable attenuation is only seen at some of the low-frequency EO buzz-saw tones. Clearly in an acoustically lined inlet duct the reduction in the buzz-saw tones will lead to an improvement in the noise levels, compared with the hard-walled inlet duct. However overall the benefit over the whole frequency spectrum is perhaps less than would be expected when compared with the considerable tonal noise reductions predicted at the lower (supersonic) operating speed.

Fig. 8 shows that Sarin and Rademaker measured at most about 20 dB liner insertion loss over the supersonic fan operating speeds. The measurements plotted in Fig. 8 are the mean SPLs at blade passing frequency. Sarin and Rademaker note that at the fan face the sound field is dominated by rotor-alone components (i.e., $m = \text{EO}$); however "... a non-uniform flow distribution, non-cylindrical inlet duct and intercostal hard-walled strips (note: in the acoustically lined duct) cause strong scattering of modes."

In the hard-walled inlet duct the modal scattering is confined to a small number of modes adjacent to rotor-alone. The amplitudes of the scattered modes appear comparable to the rotor-alone component. However in the acoustically lined inlet duct there is strong scattering of the

modes, and in particular when NL < 80% the amplitudes of the non-rotor-alone modes appear significantly greater than the rotor-alone component.

In general the scattered modes will be less well attenuated by the acoustic lining. Therefore when NL < 80% a significant contribution to the SPL (measured at BPF) will be from the non-rotor-alone modes.

While the current paper was in preparation Rademaker *et al.* [16] published mode detection results from a Rolls–Royce model fan rig as part of the RESOUND project. Results in Ref. [16] clearly illustrate that when the fan speed is less than about 80% NL the amplitude of the rotor-alone tone, compared with the amplitudes of the various scattered modes, is up to about 20 dB less measured at the end of the inlet duct.

In this paper FDNS predictions of the liner insertion loss for the "model" fan predict about 40 dB at the lower supersonic speed. This apparent large discrepancy with the measured insertion loss in Ref. [12] is to be expected in light of the modal measurements in Refs. [12,16]. The measured liner insertion loss at lower supersonic speeds is likely to be significantly less than predicted by FDNS which only calculates the rotor-alone pressure field.

In summary, when considering the rotor-alone and buzz-saw noise, the change in performance of this SDOF acoustic liner, with change in operating speed, appears to be the most significant factor in determining the benefit of the lining. At high speeds the predicted liner performance is poor for all frequencies other than some of the low-frequency EO buzz-saw tones. Therefore it is anticipated that at high speeds the noise reduction in a lined duct will primarily be in the buzz-saw tones. There is little benefit predicted at higher frequencies.

In a hard-walled inlet duct the dominant tones are likely to be buzz-saw, whereas in a soft-walled inlet duct the dominant tones are likely to be the BPF harmonics. These FDNS results are consistent with the observations reported in Sarin and Rademaker, and suggest a plausible explanation for the apparent reduction in liner insertion loss which has been measured at high operating speeds in aero-engine inlet ducts.

4. Conclusions

McAlpine and Fisher [11] described a numerical simulation model, termed FDNS, which was used for the prediction of the rotor-alone tones generated by an aero-engine. In most modern aero-engine inlet ducts there is an acoustic liner. In this paper FDNS is used to predict the tones generated by a supersonic fan in a lined inlet duct. The performance of a (locally reacting) perforate liner is determined by calculating the predicted *linear* attenuation of the rotor-alone modes. Then this is used in the FDNS model to calculate the non-linear propagation of an irregular sawtooth pressure signature attached to a supersonic ducted fan inside an acoustically lined aero-engine inlet duct. The number of harmonics which are calculated by FDNS(2) has been reduced by a factor of 10 compared with FDNS(1), by deriving a new "dissipation rate" ε which depends on the mode number m, the number of harmonics N and the time of flight T. This considerably reduces the computational effort required. Note that the essential physics associated with the FDNS methodology remain unchanged from Ref. [11].

The predictions obtained by using FDNS compare the EO frequency spectrum in both a hard-walled and acoustically lined inlet duct (at $M_{rel} \approx 1.2$ and 1.4). The liner performance is predicted

to change quite significantly with increasing fan operating speed. At the higher speeds there is predicted to be less reduction in the SPL of the tones with the inclusion of the liner. At these speeds the liner performance is poorer, compared with the lower supersonic speed. The liner is predicted to only significantly attenuate the low-frequency EO buzz-saw tones. For all high-frequency (> BPF) EO tones the predicted liner attenuation is low. Therefore the attenuation of the BPF tone in a hard-walled inlet duct, by non-linear interactions with the buzz-saw tones, will be comparable with the attenuation of the BPF tone in an acoustically lined inlet duct, by the lining. The liner insertion loss for the BPF tone is predicted to be small, and possibly even negative, at high fan speeds. The benefit of the liner at these higher speeds is confined to a reduction in the buzz-saw tones.

In a hard-walled inlet duct the dominant tones are predicted to be buzz-saw; in a lined duct the BPF harmonics are likely to remain to be significant tones in the EO spectrum. This is consistent with experimental observations reported in Sarin and Rademaker [12].

The calculation of the liner performance assumes the liner is uniform, and does not include any allowance for the curvature of the liner inside the inlet duct. Also the liner in an aero-engine is unlikely to be in one section. There will be hard axial strips between segments of the liner. This may lead to the generation of "liner scattered" tones. These are similar to "interaction" tones, where the modes are scattered out of rotor-alone, and may be poorly attenuated by the liner, compared with the rotor-alone modes. Therefore by the end of the lined inlet duct the dominant tones may not be rotor-alone. (Sarin and Rademaker have shown that the rotor-alone modes may not be the dominant modal content by the end of the inlet duct.)

The FDNS model requires further comparison with experimental measurements from an acoustically lined inlet duct in order to ascertain the accuracy of this prediction method. However this model provides a simple approach to the problem of noise prediction for a supersonic ducted fan in an aero-engine. Further work is required to assess the noise sources in a lined duct, in order to determine whether the rotor-alone tones will be the dominant noise source. Preliminary results in this paper suggest that an acoustic lining in an aero-engine inlet duct is likely to reduce the buzz-saw noise, but not necessarily the BPF tonal noise.

Acknowledgements

The authors wish to thank Dr. B.J. Tester (Rolls–Royce plc) for his contribution to this work on the RESOUND project, and for his detailed comments on an earlier draft of this paper.

We also thank Dr. E.R. Rademaker (NLR Amsterdam) for his contribution to this work on the DUCAT project, and for the provision of experimental data originally reported in Sarin and Rademaker [12].

The work was funded by the European Community X-noise research projects RESOUND and DUCAT. The support of Mr. P. Kruppa (Technical Monitor for the Commission) is particularly acknowledged.

One of us (MJF) wishes to acknowledge the continuing financial support provided by Rolls–Royce plc.

Appendix A. Calculation of *linear* modal attenuation rates in an acoustically lined cylindrical duct

Currently the predicted *linear* attenuation, at each EO, is calculated by using linear duct acoustics theory. For a cylindrical duct containing a uniform axial flow M_a, (see Fig. 2), a harmonic noise source (with frequency ω) is introduced into the duct, resulting in a harmonic pressure field $p(r,\theta,z,t)=\hat{p}(r,\theta,z)\exp(\mathrm{i}\omega t)$ which satisfies the convected Helmholtz equation

$$(\mathrm{i}k+M_a\,\partial/\partial z)^2\hat{p}=\nabla^2\hat{p}. \tag{A.1}$$

It is well known (e.g., Ref. [17]) that on separating the variables r, θ and z a modal solution of Eq. (A.1) will be of the form

$$\hat{p}_{mn}(r,\theta,z)=A_{mn}\mathrm{J}_m(\kappa_{mn}r)\exp[\mathrm{i}(-k_z z\pm m\theta)], \tag{A.2}$$

where

$$k_z=\frac{k}{(1-M_a^2)}\left[-M_a\pm\left\{1-(1-M_a^2)\left(\frac{\kappa_{mn}}{k}\right)^2\right\}^{1/2}\right], \tag{A.3}$$

m and n are integers, A_{mn} is a constant and J_m is the Bessel function of the first kind of order m. Modal solution (A.2) has azimuthal and axial wavenumber m and k_z, respectively, and radial eigenvalues denoted by κ_{mn}.

The boundary condition for a duct of radius b with a locally reacting wall with (non-dimensional) specific acoustic impedance Z reduces to the eigenvalue problem:

$$\kappa_{mn}b\,\mathrm{J}'_m(\kappa_{mn}b)/\mathrm{J}_m(\kappa_{mn}b)=-\mathrm{i}kbA(1-M_ak_z/k)^2, \tag{A.4}$$

where $A=1/Z$ is the (non-dimensional) specific acoustic admittance. (In a rigid duct $A\equiv 0$.)

From Eq. (A.2) the linear attenuation of mode (m,n) where m and n are the azimuthal and radial order, is given by

$$\partial\hat{p}_{mn}/\partial z=-\mathrm{i}k_z\hat{p}_{mn}. \tag{A.5}$$

Eq. (A.5) in terms of the non-dimensional variables (5) is equivalent to

$$\partial\hat{P}_{mn}/\partial T=-(\mathrm{i}k_zD/K)\hat{P}_{mn}, \tag{A.6}$$

where K is defined by Eq. (2). The linear attenuation rate $\sigma(m)$ (in Eq. (38)) is calculated from Eq. (A.6) by setting

$$\sigma(m)=\mathrm{Re}\{\mathrm{i}k_zD/K\}=-k_{zi}D/K, \tag{A.7}$$

where $k_z=k_{zr}+\mathrm{i}k_{zi}$ is the axial wavenumber for the least attenuated radial duct mode with azimuthal mode number m.

In Ref. [11] only the real part of $\mathrm{i}k_zD/K$ was used in FDNS(1) because this term was only used to approximate cut-off in a hard-walled inlet duct. In a soft-walled inlet duct an acoustic liner will affect both the amplitude and phase of the modes. However in this paper again only the real part of $\mathrm{i}k_zD/K$ is used in FDNS(2). This simulates the absorption properties of the acoustic lining (and at this time simplifies the problem by omitting liner phase shift effects from the prediction). In FDNS(2) with an acoustically lined inlet duct set $\sigma(m)$ to be the real part of $\mathrm{i}k_zD/K$ where for each EO m, calculate k_z for the least attenuated radial mode, typically the $(m,1)$ duct mode.

The liner absorption is calculated by three-dimensional linear duct acoustics theory. There is no radial dependence in the FDNS method. The sawtooth waveform is assumed to be located at a fixed radial distance in the inlet, nominally at the duct wall $r = b$. Therefore for each m the *linear* liner performance is predicted by the *least* attenuated radial mode. For most m this will typically be the first radial order, i.e., $n = 1$. This paper does not attempt to address questions concerning any modification to the radial sound field due to the attenuation by the acoustic lining. However one notes that while this paper was in preparation Bréard et al. [18] published some CFD-based numerical simulations of tonal noise in a lined inlet duct using a non-linear model. Fig. 9 (p. 6) in Ref. [18] shows the radial pressure field in a lined duct (at BPF) calculated by the non-linear CFD model compared with the first radial mode predicted from linear theory (i.e., Eq. (A.2) with $m = B$ and $n = 1$). The two plots appear to be in close agreement.

Finally, the (non-dimensional) specific acoustic impedance Z of the SDOF locally reacting acoustic lining is for simplicity assumed to be

$$Z = R + \mathrm{i}X_c, \tag{A.8}$$

where R is the face-sheet resistance and X_c is the cavity reactance. Motsinger and Kraft [19] suggest the following estimates for R and X_c:

$$R = 0.3M_a/\rho \quad \text{and} \quad X_c = -\cot(kh). \tag{A.9}$$

ρ is the face-sheet porosity and h is the cavity depth of the liner's honeycomb structure.

References

[1] M.G. Philpot, The buzz-saw noise generated by a high duty transonic compressor, ASME Paper No. 70-GT-54, 1970.

[2] D.L. Hawkings, Multiple tone generation by transonic compressors, Journal of Sound and Vibration 17 (1971) 241–250.

[3] M. Kurosaka, A note on multiple pure tone noise, Journal of Sound and Vibration 19 (1971) 453–462.

[4] M.R. Fink, Shock wave behaviour in transonic compressor noise generation, ASME Paper No. 71-GT-7, 1971.

[5] G.F. Pickett, Prediction of the spectral content of combination tone noise, Journal of Aircraft 9 (1972) 658–663.

[6] B.S. Stratford, D.R. Newby, A new look at the generation of Buzz-saw noise, AIAA 77-1343, 1977.

[7] P. Sijtsma, Prevention of Buzz-saw noise by acoustic lining, in: CEAS/AIAA-95-077, First Joint CEAS/AIAA Aeroacoustics Conference, Munich, Germany, June 12–15, 1995, pp. 575–583.

[8] P. Gliebe, R. Mani, H. Shin, B. Mitchell, G. Ashford, S. Salamah, S. Connell, Aeroacoustic prediction codes, Technical Report NASA CR-2000-210244, NASA Glenn Research Center, 2000, 323pp.

[9] C.L. Morfey, M.J. Fisher, Shock-wave radiation from a supersonic ducted rotor, The Aeronautical Journal of the Royal Aeronautical Society 74 (1970) 579–585.

[10] M.J. Fisher, B.J. Tester, P.J.G. Schwaller, Supersonic fan tone noise prediction, AIAA 98-2249, 1998.

[11] A. McAlpine, M.J. Fisher, On the prediction of "Buzz-saw" noise in aero-engine inlet ducts, Journal of Sound and Vibration 248 (1) (2001) 123–149.

[12] S.L. Sarin, E.R. Rademaker, In-flight acoustic mode measurements in the turbofan engine inlet of Fokker 100 aircraft, AIAA 93-4414, 1993.

[13] D.G. Crighton, A.P. Dowling, J.E. Ffowcs Williams, M. Heckl, F.G. Leppington, Modern Methods in Analytical Acoustics, Springer, Berlin, 1992.

[14] G.B. Whitham, Linear and Nonlinear Waves, Wiley, New York, 1974.

[15] Yu.A. Pishchal'nikov, O.A. Sapozhnikov, V.A. Khokhlova, A modification of the spectral description of nonlinear acoustic waves with discontinuities, Acoustic Physics 42 (1996) 362–367.

[16] E.R. Rademaker, P. Sijtsma, B.J. Tester, Mode detection with an optimised array in a model turbofan engine intake at varying shaft speeds, in: AIAA 2001-2181, Proceedings of the Seventh AIAA/CEAS Aeroacoustics Conference & Exhibit, Maastricht, The Netherlands, May 28–30, 2001.
[17] W. Eversman, Theoretical models for duct acoustic propagation and radiation, in: H.H. Hubbard (Ed.), Aeroacoustics of Flight Vehicles: Theory and Practice, Vol. 2, Noise Control, NASA RP-1258, 1991, pp. 101–163.
[18] C. Bréard, A. Sayma, M. Imregun, A.G. Wilson, B.J. Tester, A CFD-based non-linear model for the prediction of tone noise in lined ducts, in: AIAA 2001-2176, Proceedings of the Seventh AIAA/CEAS Aeroacoustics Conference & Exhibit, Maastricht, The Netherlands, May 28–30, 2001.
[19] R.E. Motsinger, R.E. Kraft, Design and performance of duct acoustic treatment, in: H.H. Hubbard (Ed.), Aeroacoustics of Flight Vehicles: Theory and Practice, Vol. 2, Noise Control, NASA RP-1258, 1991, pp. 165–206.